Authors' manuscript
Article published in *NDT & E International* Volume 103, April 2019, Pages 119-129
https://doi.org/10.1016/j.ndteint.2019.02.007

# DESIGN AND OPTIMISATION OF A PHASED ARRAY TRANSDUCER FOR ULTRASONIC INSPECTION OF LARGE FORGED STEEL INGOTS

Frederic Dupont-Marillia[1,a)], Mohammad Jahazi[1,b)], Serge Lafrenier[2,c)], Pierre Belanger[1,d)]

[1] *Department of mechanical engineering, École de technologie supérieure, 1100 rue Notre-Dame Ouest, Montreal, Quebec, Canada*

[2] *Finkl Steel Sorel, 100 Rue McCarthy Saint-Joseph-de-Sorel, Canada*

[a)]Corresponding author: Frederic.dupont.1@ens.etsmtl.ca
[b)]mohammad.jahazi@etsmtl.ca
[c)] slafreniere@finkl.com
[d)]pierre.belanger@etsmtl.ca



## Abstract

Large steel forgings are used in numerous industries. This paper investigates the possibility of adapting ultrasonic phased array testing to the inspection of forged steel blocks with dimensions of up to 1000 mm in every direction. The paper looks at two objectives in order to provide the best inspection performance: (1) the ultrasonic phased array probe optimisation and (2) the ultrasonic wave transmission sequence in a total focusing method imaging scenario. The CIVA software suite was used to optimize the phased array probe element count and width in a full matrix capture configuration. Based on the simulation results, a 32-element transducer was then built and tested in a 777 mm forged steel block using full matrix capture, plane wave and Hadamard transmission sequences. It was observed that plane wave and Hadamard sequences transmit significantly more energy inside the test sample because the elements are emitting simultaneously, therefore leading to an improved signal-to-noise ratio. However, the horizontal resolution was a strong limitation for every transmission sequence, especially for plane waves, because of the limited range of angles available in a block of large dimensions. The Hadamard transmission sequence was shown to represent the best compromise in terms of defect reflected amplitude, signal-to-noise ratio and resolution. The experimental results were compared with simulations and were found to be in very good agreement.

**Keywords:** Phased array; large size; forged steel; Full Matrix Capture; Plane Wave; Hadamard; Imaging;

## Introduction

Ultrasonic waves have been used for over 60 years in the medical and industrial fields. Ultrasonic testing (UT) is the most widely used non-destructive testing (NDT) method to inspect parts, measure dimensions and evaluate material properties. More recently, phased array ultrasonic testing (PAUT) was developed to generate images of parts under inspection, and has demonstrated many advantages in terms of probability of detection and inspection cost [1]. Over the past decade, PAUT has been applied to ensure the quality of safety-critical components in the aerospace, power generation and oil and gas industries. Indeed, ultrasonic imaging allows the visualisation of cracks, porosities or other subsurface defects of test specimens. Nowadays, the research community is moving its focus to increasing the image reconstruction rate [2], precision and signal-to-noise ratio (SNR) [3], as well as inspecting more complex components such as those made of highly attenuating materials [4] and anisotropic materials [5]. In some particular applications, e.g., automotive injection moulding, large forged steel blocks are produced, and their NDT is of significant concern because of the long propagation distances associated with the dimensions of the blocks, which lead to strong signal attenuation. Moreover, defects located close to the centre of the block are of high interest since they may correspond to moulding surfaces.

This paper thus investigates the ultrasonic imaging of large steel forgings (more than 1000 mm in every direction) from (1) the probe design and (2) the wave transmission sequence. Conventional commercially available PAUT probes are typically not powerful enough to generate ultrasonic waves with enough energy to detect defects or other heterogeneities at distances up to 1000 mm because of the small dimensions of the piezoelectric elements involved. In that context, single element transducers with large diameters (usually more than 25 mm) are still preferred because imaging of large blocks remains too challenging. For these reasons, an adapted probe and several transmission sequences were studied to improve PAUT imaging in large forged steel blocks.

The aim in this study is to maximise the energy transmitted into the block without sacrificing the image resolution or the probability of detection of typical defects. The first part of this paper focuses on the probe design. Probe properties such as the element count, the element width and the aperture were studied in order to evaluate their influence on the energy transmitted into the test sample, as well as the imaging sensitivity and resolution. The second part of the paper investigates alternative wave transmission sequences. Today, the total focusing method (TFM) [6] with the full matrix capture (FMC) [7] wave transmission sequence is of great interest for industries because it allows a wide range of inspections and an easy imaging reconstruction process. Other methods studied in this paper include the transmission of plane waves (PW) [8] generated from the simultaneous activation of multiple elements following a delay law to create plane wavefronts. Finally, a new approach is proposed using a Hadamard matrix for generating transmission sequences. This novel method represents a compromise between FMC and plane wave transmission for energy transmission and SNR. The Hadamard transmission sequence combines high-energy waves generated from the simultaneous activation of multiple elements and the acquisition on all element combinations similar to FMC.

This article begins with a review of the scientific background relevant to this paper. The design and optimisation of the PAUT probe are then presented in simulations. Experimental validations of the PAUT probe and the transmission sequences are then presented and discussed. Finally, conclusions are drawn.

## Wave Transmission Sequences

PAUT requires a probe that can transmit and receive on multiple elements organised in a one- or two-dimensional matrix. The present work only considers one-dimensional linear arrays. Over the years, several methods have been proposed for element activation, leading to a range of different reconstruction algorithms. In the context of the PAUT of a large block, the conventional beam focusing technique does not appear to be adapted because of the time required to focus ultrasonic waves over a very large area. Therefore, the present work compares images obtained through three different transmission sequences: (1) FMC, (2) PW and (3) the Hadamard matrix. Background information on the three methods are detailed in the following subsections.

- **Full Matrix Capture**

FMC [7] performs the acquisition of M = N x N signals corresponding to all pairs of elements in a probe. This sequence has the advantage of being relatively simple to implement since no delay laws are required. A schematic of the FMC sequence is shown in Figure 1.

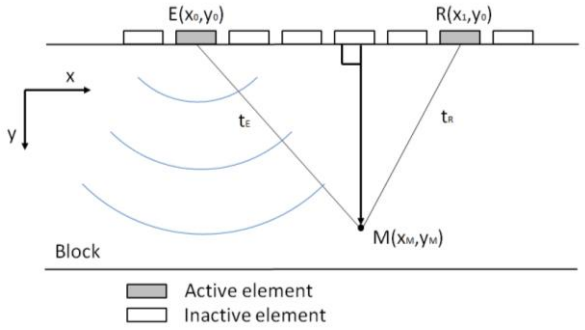


Figure 1: Schematic of the Full Matrix Capture wave transmission sequence

Reconstruction is performed by coherently summing all signals $S_{NM}$ for each pixel $i$ and $j$ of the image matrix using the following equation:

$$A_{NM} = \left| H\left( \sum_{N=1}^{N} \sum_{N=1}^{M} S_{NM}(t_E + t_R) \right) \right| \quad (1)$$

where $H$ is the Hilbert transform [9], $t_E$ is the time of flight between the emitter $E$ and the pixel of interest $(x_M, y_M)$, $t_R$ is the time of flight between the receiver $R$ and the pixel of interest and $V_L$ is the longitudinal speed of sound:

$$t_E = \sqrt{(x_M - x_0)^2 + (y_M - y_0)^2} \Big/ V_L \quad (2)$$

$$t_R = \sqrt{(x_M - x_1)^2 + (y_M - y_0)^2} \Big/ V_L \quad (3)$$

- **Plane Wave Transmission**

PW imaging was recently proposed in order to improve the frame rate and the SNR [8]. This method activates all elements at each transmission in order to generate a coherent plane wavefront defined by the angle α relative to the propagation axis. The energy transmitted into the material is higher than for FMC, and SNR is therefore increased. Contrary to FMC, for which the number of transmissions depends on the number of elements, in PW imaging, the number of transmissions is defined by the number of angles (generally set between 10 and 30). This low number of transmissions therefore leads to high frame rate imaging [3], [10]. With PW, the resolution mainly depends on the path differences introduced by the different angles. In the context of the inspection of blocks of large dimensions, the angular range is limited by the geometry associated with the long propagation distances involved. A schematic of the PW transmission and acquisition sequence in presented in Figure 2.

The coherent signal summation for image reconstruction also uses equation (1) from the subsection above. The time of flight between the pixel of interest and a receiver $(t_R)$ remain unchanged from equation (2), but the time of flight between an emitter and the pixel of interest $(t_E)$ depends on the wavefront angle, and can be found with:

$$t_E = \frac{(x_M - x_0)\ \sin\alpha + \ (y_M - y_0)\cos\alpha}{V_L} \quad (4)$$

- **Hadamard Matrix Transmission**

This transmission method is a succession of multiple element activations following a Hadamard matrix sequence. This method varies the synthetic transmit aperture (STA), and thus, the amount of energy transmitted into the material. This technique has demonstrated very good results by increasing SNR [11]. In the present work, a new transmission method was investigated, and is a combination of PW and Hadamard transmission. The objective was to perform different acquisitions, varying from PW transmission, where all elements are activated simultaneously, leading to a maximum transmitted energy to FMC transmission on a single element, and therefore, to a lower transmitted energy, but a better resolution. Hadamard sequences are presented for an 8-element transducer in Figure 3.

The reconstruction algorithm is based on a combination of time-of-flight calculations, as in FMC and PW. If the pixel to be reconstructed is located inside the sequence's active aperture zone, then the time of flight is provided by equation (4) from PW, otherwise the FMC time of flight in equation (2) is used. In both cases, the pixel-to-receiver distance remains unchanged, and can be found using equation (3). A schematic of the active aperture

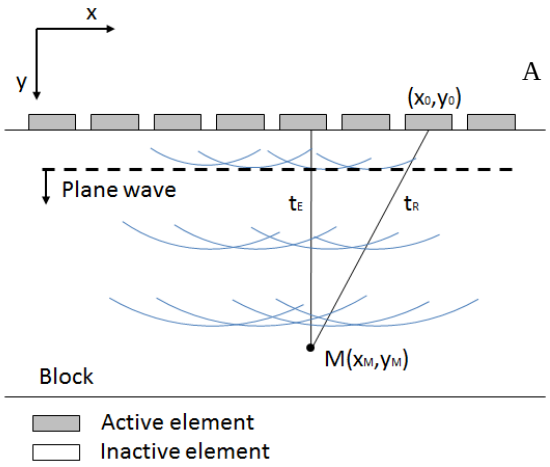


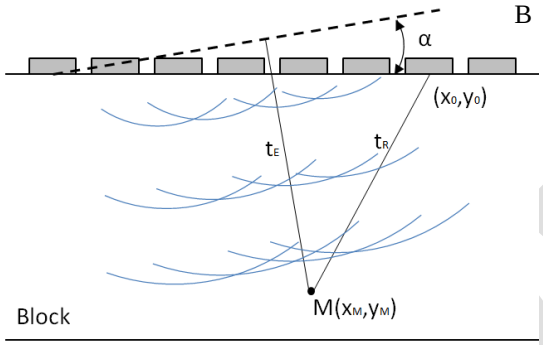


Figure 2: Schematic of plane wave transmission at 0° (A) and $\alpha$ ($B$) angles

zone for the Hadamard matrix transmission is presented in Figure 4 when 2 elements are grouped together.

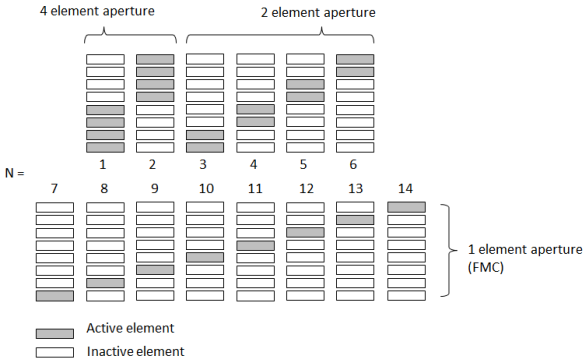


Figure 3: Hadamard matrix transmission sequence

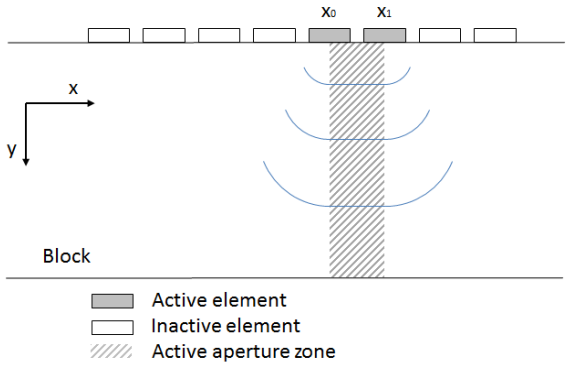


Figure 4: Active aperture in the Hadamard matrix transmission sequence. The figure shows the case of 2 elements grouped together.

## Transducer Design

- **Modelling**

Modelling was performed with the CIVA UT simulation package [12], a specialised NDT simulation platform. In the present work, a 1000 mm thick block was simulated using parameters obtained from measurements performed on a similar block in a previous study by our team [13]. The aim of this work was also to evaluate the anisotropy of the material from an ultrasonic point of view. Strong anisotropy would lead to deterioration of the image quality. It was observed that along the inspection axis the velocity variations were under 0.1%. In order to study imaging capabilities at different depths, simulations of circular defects were performed for defect depths varying between 50 mm and 900 mm. A 2.25 MHz center frequency was used. It corresponds to the typical inspection frequency recommended by ASME for the inspection of these large parts using conventional UT. The PAUT probe parameters, such as the element number and width, were also varied in order to study the effect of the aperture on the defect-reflected amplitude and the resolution. To this end, the element width was chosen to vary from 1 mm (close to the largest commercially available probes) to 20 mm. The probe design was performed with the FMC emission sequence because of its limited energy transmitted into the material, as compared with PW or Hadamard matrix transmission sequences. Simulations were performed in two dimensions and without noise for computing time reasons.

- **Simulations**

A total of 375 simulations and TFM reconstructions were performed for 8, 16, 32, 64 and 128 elements to evaluate the influence of the element width and the number of elements on the reconstructed defect amplitude and resolution of a 1.59 mm diameter defect, as a function of depth. Horizontal and vertical resolutions were taken as the full width at half maximum (eq. -6 dB) of the defect along the x- and y-axes, respectively. Each defect amplitude was normalised for all simulations with the maximum amplitude of all simulations in order to allow direct comparisons between them. As the amount of data generated for each image is consequent especially considering the recording time linked with the dimensions (even using a low sampling) the number of elements was a strong concern. For this reason, the data are displayed for different element number as a function of size and depth. First, the amplitudes were extracted, and results are presented in Figure 5. For the sake of brevity, only 16 (A), 32 (B), 64 (C), and 128 (D) elements are shown. With elements of a width of 1 mm, the amplitude decreased faster than for any other dimensions between depths of 50 mm and 900 mm. Amplitude losses of 70 dB, 70 dB, 65 dB, and 55 dB were respectively observed for 16, 32, 64, and 128 elements. The plots therefore show that conventional probes are not adapted to the inspection of large forged ingots because the transmitted amplitude is too low, and the ultrasonic field is not focused adequately with the dimensions. This result thus confirms that a new probe design was required. By analysing the trend of the curves for elements wider than 1 mm, it was observed that increasing the element number reduces the amplitude loss. For a low number of elements, the width did not appear to have a strong influence on the amplitude, but for 64 and 128 elements, smaller elements provided higher amplitudes, especially for low propagation distances. In order to provide more information, the vertical resolution was then computed, and results are presented in Figure 6. According to these simulations, the vertical resolution appeared to be below 10 mm. Considering the size of the ingots this study aimed to inspect, this value seemed to be low, and was not considered as a limitation for the transducer design. Some data were removed in Figure 6C (for 20 mm) and Figure 6D (for 15.2 mm and 20 mm) widths.

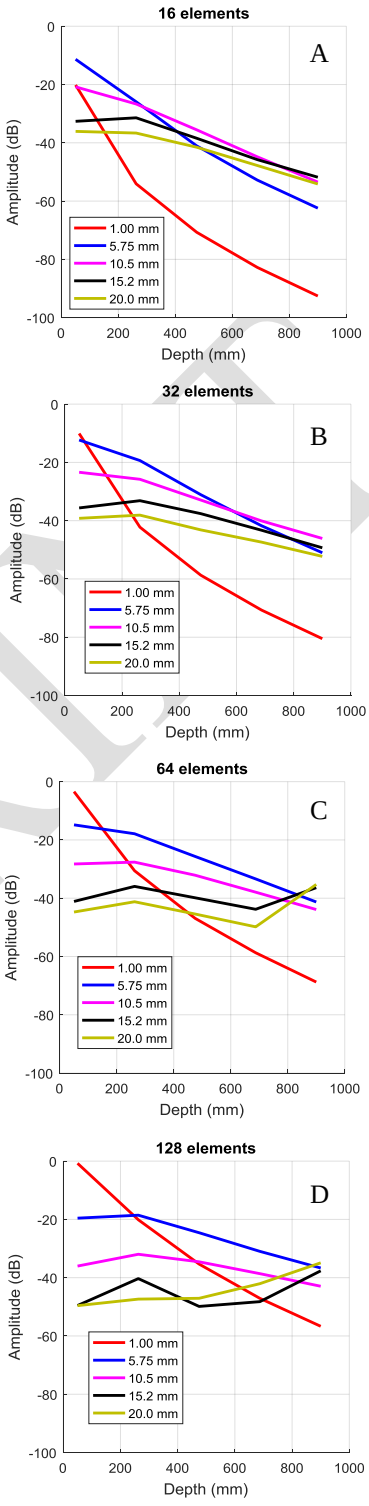


Figure 5: Amplitude over depth from simulations of a 1.59 mm defect after TFM reconstruction as a function of the element number and width A: 16 elements, B: 32 elements, C: 64 elements, and D: 128 elements

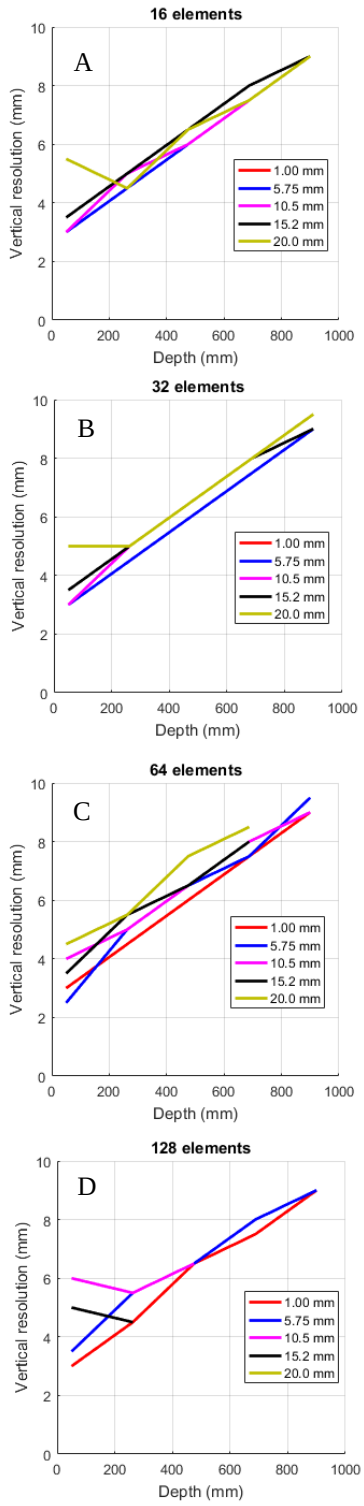


Figure 6: Vertical resolution over depth from simulations of a 1.59 mm defect after TFM reconstruction as a function of the element number and width (A: 16 elements, B: 32 elements, C: 64 elements, and D: 128 elements)

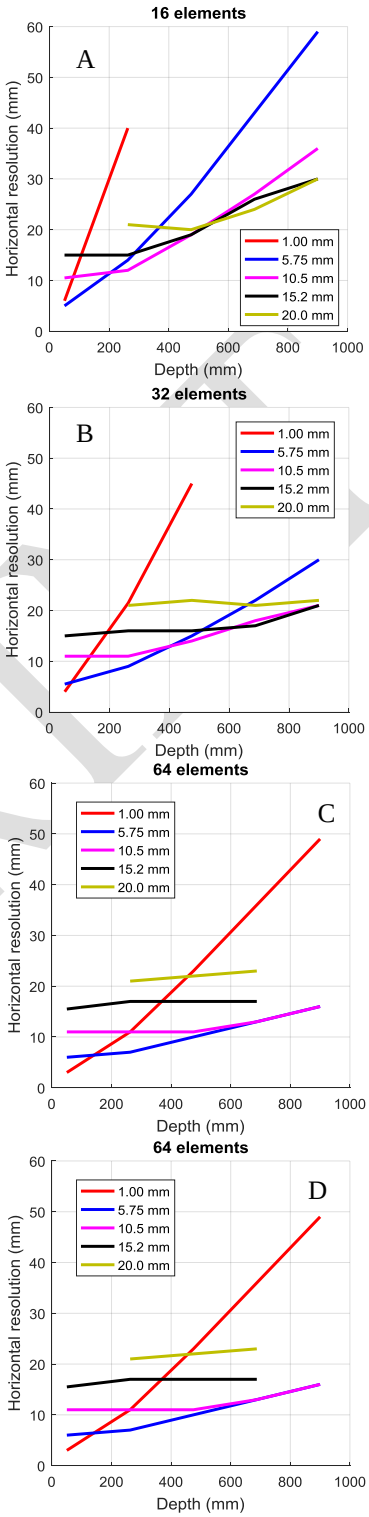


Figure 7: Lateral resolution over depth form simulations of a 1.587 mm defect after TFM reconstruction as a function of the element; A: 16 elements, B: 32 elements, C: 64 elements, and D: 128 elements

The results were rejected because strong artefacts were generated in these cases. Indeed, for some particular probe configurations with more than 64 elements with widths of 15.2 mm and greater, artefacts strongly decreasing the image quality. These artefacts are associated with constructive interferences which can be removed by selecting data based on the angle between emission and reception [14]. Finally, the lateral resolution was extracted and analysed following the same procedure, and results are presented in Figure 7.

Data points were rejected for 64 and 128 elements at 20 mm and 15.2 mm, respectively. The same artefacts observed previously degraded the images and the resolution value. Compared to the vertical resolution ( Figure 6), the lateral resolution appeared to be between 2.5 and 6 times higher. These high values showed that the imaging quality would be limited by the lateral resolution. In addition, it was observed that increasing the element number improves the resolution. At high depths, an element width between 5 mm and 15 mm appeared to offer the best resolution.

Finally, using the amplitudes and resolutions that were computed and extracted appeared to indicate that the best configuration would be 32 elements with a width of 9.25 mm.

## Experiments

Experiments were conducted on a large block of forged steel with artificial defects, such as side drilled holes and notches, at different depths.

- **Material**

The block used for this work was a high-strength steel block with a thickness of more than 760 mm, which was forged and heat treated. The block was machined on one side with 3 flat notches oriented perpendicular to the inspection axis at a depth of 184 mm, 406 mm and 611 mm. On the other side, 3 circular defects of around 10 mm were drilled: a 6.35 mm diameter hole at a depth of 368 mm, a 3.18 mm diameter hole at a depth of 372 mm, and finally, a 1.59 mm diameter hole at a depth of 366 mm. This configuration is presented in Figure 8. A previous study conducted on a similar block produced with the same manufacturing process at the same plant provided metallurgical and ultrasonic measurements for the simulations [15]. This block was mainly bainitic (98

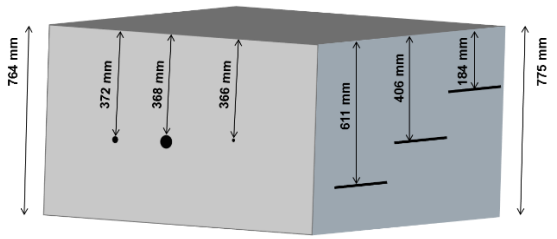


Figure 8: Schematic of the block used in the experimental validation

-99%) with residual austenite (±1%); the density was 7950 kg/m$^3$, and the ultrasonic longitudinal and shear velocities were respectively 5930 m/s and 3230 m/s. Attenuation along the propagation axis was 0.08 dB/mm for a 2 MHz frequency, with a power growth factor of 2. This value is consistent with the one from literature [16].

- **Measurement Setup**

A custom PAUT probe was built according to the simulations with 32 PZT IV elements with a width of 9.25 mm (which was the nearest commercially available size with would give a pitch close to 10.5 mm including a 1 mm spacing from the 3D printer spacers). The element length was not computed because simulations were done with a 2D model due to the computational cost associated with a 3D model. However the element length was determined using the relationship between the width to length ratio for rectangular elements and the near field depth [17]. The ratio used for the element length to the element width was 0.4, leading to a 22.5 mm element length. This design minimises the near field and maximise the amplitude of the ultrasonic field. This method is commonly used by the manufacturer for probe design. The element thickness was set to 1.1 mm to obtain a 2.4 MHz resonant frequency. Measurements were performed with a Verasonics Vantage 64 LE at 2.4 MHz, with 80% bandwidth signals, and data were post-processed using MatLab. The full setup is presented in Figure 9.

Figure 9: Experimental setup

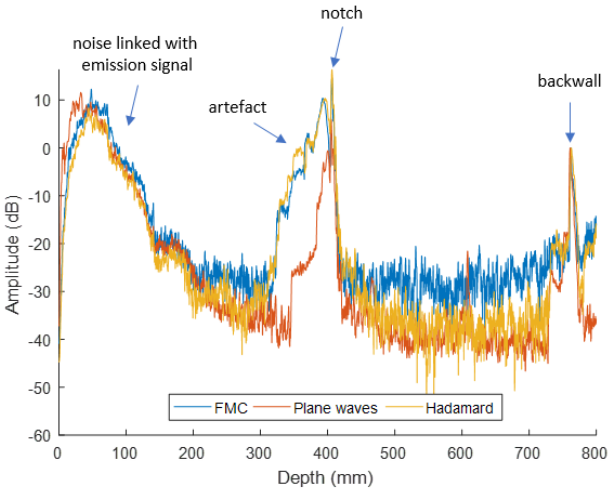


Figure 10: Experimental vertical profile from 406 mm depth notch images for FMC, PW and Hadamard matrix transmission sequences

## Imaging with FMC, PW and Hadamard Matrix Transmission Sequences

The following section presents the results from the measurements made on the steel block with the experimental probe presented above. All parameters such as amplitudes and resolutions were extracted following the same process and algorithm used for simulations. Measurements averaging was set to 256.

### Imaging of Notches

The first measurements were performed on the 3 notches located at depths of 184 mm, 406 mm and 611 mm. The reconstructed images for FMC, PW and Hadamard matrix transmission sequences are presented in Appendix A. Vertical profiles were extracted and compared for the 3 transmission sequences. As an example, Figure 10 presents the vertical profiles for the notch at 406 mm. The vertical profiles show 2 peaks linked with the notch (406 mm depth) and the backwall. High amplitude noise decreased image quality down to approximately a depth of 150 mm. This noise was a consequence of high electromagnetic noise due to a power transformer in the close vicinity of the block, as well as poor absorption from the backing layer of the probe.The profiles were normalised to the amplitude of the backwall echo. It also appeared that the noise floor was higher for FMC. SNR and notch position accuracy was extracted and compared. The accuracy is given as a percentage of the error in the position between the reconstructed notch and the true measurement made on the block divided by the true distance. SNR is the difference of amplitude between the notch maximum amplitude and the surrounding noise floor. Accuracy and SNR are presented for the 3 emission sequences and the 3 notches in Figure 11. The error on the notch positions appeared to be very low (below 1.2%), considering the measurement uncertainties and the velocity variation (0.85% [13]). It is also noteworthy that the images from FMC sequences seemed to be more affected by velocity variation, with errors increasing with the distance of propagation.

The SNR levels were higher than 30 dB for every emission sequence, which allowed an easy visualisation of the notches. For the three configurations, the SNR seemed to increase up to a maximum value, which was a function of the number of elements reaching the notch for an emission. Indeed, Hadamard matrix and PW transmission sequences that both generate waves by simultaneously activating multiple elements have similar maximum SNR, which is 9 dB higher than FMC. After this maximum, the SNR decreases due to attenuation. In order to have the best probe design, the parameters (element size and number) which gave to the best SNR at 500mm depth were chosen. As the design is not optimal before this depth, the sensitivity is lower. Then the SNR depend on this sensitivity and on the noise floor. For low distances, the noise is linked with

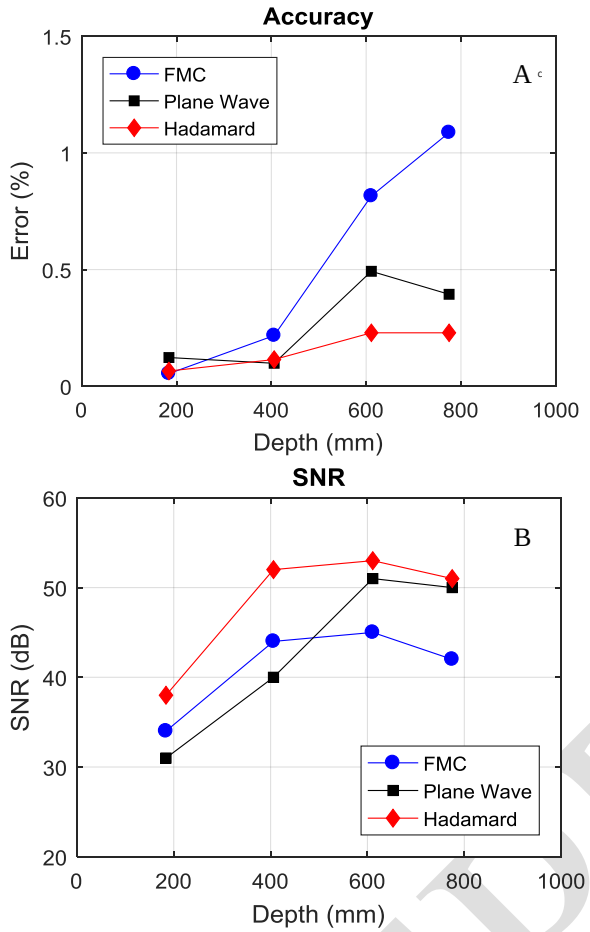


Figure 11: Experimental notch position accuracy (A) and Signal-to-Noise Ratio (B) for PAUT imaging using FMC, PW and the Hadammard matrix transmission sequences

the material scattering. As the material remains similar, SNR increase with sensitivity. For the longer distances, noise increase because of electronic noise introduced by the acquisition setup leading to an SNR decrease (also linked to UT beam amplitude decreasing).

It is interesting to note that the notch profiles are very similar for FMC and the Hadamard matrix transmission sequences, with more noise in the FMC profile. Indeed, FMC sequences transmit a lower amount of energy into the material, which results in a lower backwall amplitude as compared to the noise floor. As the backwall is set as the 0 dB reference, noise appears higher as compared to other transmission sequences. It therefore seems that the Hadamard matrix transmission sequence generates similar results as FMC, with more energy due to the grouping of the elements during transmission. From these results, it could be observed that the Hadamard matrix transmission sequence is of great interest when inspecting parts with high attenuation due to the dimensions or material properties because of the resulting better SNR. This sequence also had a lower acquisition rate due to the high number of sequences required to complete the transmission. PW also provided good SNR performances, and had the significant advantage of modifying the number of angles to optimise the image as a function of the distance. The advantages of PW over FMC consist of a better SNR for long propagation distances and a higher acquisition rate.

This experimental configuration did not allow a measurement of the resolution because the reflectors were too large. The circular defects on the other face of the block were used to that end.

- **Circular Defect Imaging**

In this section, measurements were performed on three circular defects with diameters of 1.59 mm, 3.17 and 6.35 mm at a depth of 370 mm in a 777 mm thick block. Images from FMC, PW and Hadamard matrix transmission sequences were reconstructed, and the amplitude and resolutions extracted. The amplitudes were compared using the backwall echo as a reference. Resolutions were measured along the vertical and horizontal axes at -6 dB from the defect maximum amplitude. Results were then compared with simulations and are presented in Figure 12.

The amplitudes from the three sequences follow the same trends in experiments and simulations. The reflected amplitude from the defect is the highest relative to the backwall when using FMC. This is simply an indication that the backwall echo is proportionally lower than for PW and the Hadamard matrix transmission. The Hadamard matrix transmission and FMC use similar activation patterns based on triangulation between the source, the pixel and the receiver. However, when using the Hadamard matrix transmission, multiple elements may be grouped together during the emission. The reflected amplitude from the defect is a function of the incident energy, which is directly correlated to the energy transmitted inside the material by the probe. This result therefore confirms that the Hadamard matrix transmission method transmits more energy inside the specimen under inspection than does FMC. When using PW, angled

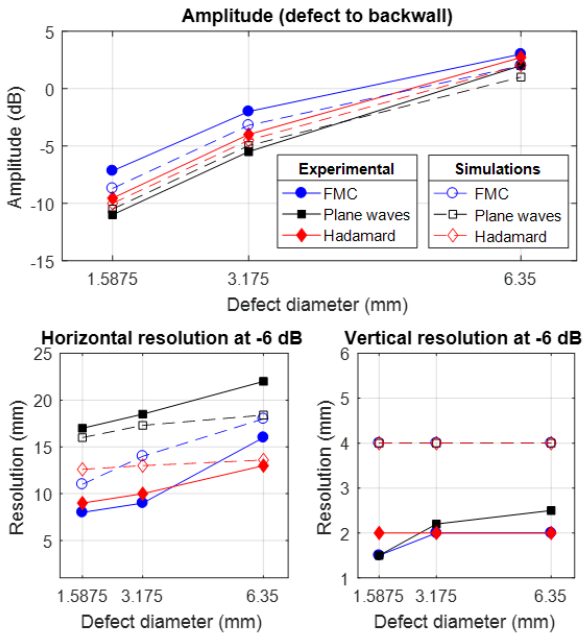


Figure 12: Comparison of amplitude (A), horizontal resolution (B) and vertical resolution (C) for imaging of circular defects at 370 mm depth using FMC, PW and Hadamard matrix transmission sequences

plane wavefronts impinging the backwall or a defect are reflected away from the probe. At ±5°, the distance between the centre point of the emitted and reflected wavefronts is 135 mm, for a backwall distance of 777 mm. This distance between emission and reception is the limit of the current probe aperture. The consequence is that the backwall amplitude is reduced as a function of the angle. In experiments, the defects were located at a depth of 370 mm, leading to a distance of 64 mm. The wave packet reflected by the defect was thus completely captured by the probe. Therefore, when using the backwall as the reference amplitude, the relative amplitude of a defect appears higher than for FMC or the Hadamard matrix transmission sequence. However, for FMC, PW and Hadamard matrix transmissions, the amplitudes between defects and the backwall appeared to be in very good agreement with simulations. For the three sequences, the resolutions were better than in the simulations along all directions, except for the horizontal resolution of PW imaging. Indeed, small differences between the angles lead to very close propagation paths between the different emissions, and therefore, to poor information on the defect location. Increasing the angular range would be of great interest, but would also decrease the resolution and amplitude of deeper defects. Since this limitation is associated with the dimensions of the blocks, it appeared that PW imaging is not a good candidate for PAUT of very large parts. Images from FMC and Hadamard sequences provided better horizontal resolutions, varying between 9 mm and 16 mm, and increasing with the defect diameter. Finally, the vertical resolution was 2.5 mm and 37.5% lower than expected from the simulations.

## Conclusions

This paper explored the possibilities of PAUT imaging of large forged steel parts. Modelling done with CIVA UT simulation software showed that PAUT probes which are typically available commercially, with elements of the order of a few millimetres, were not adapted because of the limited energy transmitted into the part under inspection. The main constraint was to design the probe aperture in order to maximise amplitude without decreasing the resolution. It was shown that for a 1000 mm block, elements of 10 mm x 22.5 mm represented a good compromise. Also, when increasing the number of elements, imaging artefacts were introduced due to constructive interference at high propagation angles. A custom PAUT probe was built with 32 elements and then used to perform imaging on a 777 mm forged steel block. The experiments were conducted on notches and circular defects using FMC, PW and Hadamard matrix transmission sequences. Results were compared in terms of amplitude, horizontal and vertical resolutions and SNR. Horizontal resolution was a strong limitation for the imaging of large size forged steel. The PW transmission sequence transmits higher energy. This is beneficial for SNR, but the resolution was worse than for FMC. Angled wavefront were varied from -5° to +5° in order to reach a compromise between surface and backwall inspection angles. In addition, the Hadamard matrix transmission sequence, which has the disadvantage of a low acquisition rate, provided very good results, with a similar resolution to that of FMC, as well as an increased amplitude and SNR. These results were compared with simulations, and a very good agreement was observed. To increase imaging capabilities, it would be of great interest to implement new reconstruction algorithms such as multi-modal TFM imaging [18] or to perform similar measurements with coded excitations such as Golay codes [19] or the chirp pulse [20].

## References


[1] B. W. Drinkwater and P. D. Wilcox, "Ultrasonic arrays for non-destructive evaluation: A review," *NDT & E International*, vol. 39, no. 7, pp. 525–541, Oct. 2006.

[2] P. Gong, P. Song, and S. Chen, "Ultrafast Synthetic Transmit Aperture Imaging Using Hadamard-Encoded Virtual Sources With Overlapping Sub-Apertures," *IEEE Transactions on Medical Imaging*, vol. 36, no. 6, pp. 1372–1381, June 2017.

[3] E. Tiran *et al.*, "Multiplane wave imaging increases signal-to-noise ratio in ultrafast ultrasound imaging," *Physics in Medicine and Biology*, vol. 60, no. 21, pp. 8549–8566, Nov. 2015.

[4] E. L. Villaverde, S. Robert, and C. Prada, "Ultrasonic Imaging in Highly Attenuating Materials With Hadamard Codes and the Decomposition of the Time Reversal Operator," *IEEE Transactions on Ultrasonics, Ferroelectrics, and Frequency Control*, vol. 64, no. 9, pp. 1336–1344, Sep. 2017.

[5] G. Ribay, C. Poidevin, G. Rougeron, and B. C. L. de Roumilly, "UT Data Reconstruction in Anisotropic and Heterogenous Welds," presented at the 8th International Conference on NDE in Relation to Structural Integrity for Nuclear and Pressurised Components Abstracts, 2010.

[6] C. Holmes, B. Drinkwater, and P. Wilcox, "The post-processing of ultrasonic array data using the total focusing method," *Insight-Non-Destructive Testing and Condition Monitoring*, vol. 46, no. 11, pp. 677–680, 2004.

[7] R. Long, J. Russell, and P. Cawley, "Ultrasonic phased array inspection using full matrix capture," *Insight - Non-Destructive Testing and Condition Monitoring*, vol. 54, no. 7, pp. 380–385, Jul. 2012.

[8] L. Le Jeune, S. Robert, E. Lopez Villaverde, and C. Prada, "Plane Wave Imaging for ultrasonic non-destructive testing: Generalization to multimodal imaging," *Ultrasonics*, vol. 64, pp. 128–138, Jan. 2016.

[9] C. Holmes, B. W. Drinkwater, and P. D. Wilcox, "Post-processing of the full matrix of ultrasonic transmit–receive array data for non-destructive evaluation," *NDT & E International*, vol. 38, no. 8, pp. 701–711, Dec. 2005.

[10] G. Montaldo, M. Tanter, J. Bercoff, N. Benech, and M. Fink, "Coherent plane-wave compounding for very high frame rate ultrasonography and transient elastography," *IEEE Transactions on Ultrasonics, Ferroelectrics and Frequency Control*, vol. 56, no. 3, pp. 489–506, Mar. 2009.

[11] I. Trots, A. Nowicki, and M. Lewandowski, "Synthetic transmit aperture in ultrasound imaging," *Archives of Acoustics*, vol. 34, no. 4, pp. 685–695, 2009.

[12] P. Calmon, S. Mahaut, S. Chatillon, and R. Raillon, "CIVA: An expertise platform for simulation and processing NDT data," *Ultrasonics*, vol. 44, pp. e975–e979, Dec. 2006.

[13] F. Dupont-Marillia, M. Jahazi, S. Lafreniere, and P. Belanger, "Influence of local mechanical properties of high strength steel from large size forged ingot on ultrasonic wave velocities," 2017, p. 090002.

[14] F. Dupont-Marillia, M. Jahazi, and P. Belanger, "Phased array inspection of large size forged steel parts," *AIP Conference Proceedings*, vol. 1949, no. 1, p. 080004, Apr. 2018.

[15] A. Loucif, E. Ben Fredj, M. Jahazi, L.-P. Lapierre-Boire, R. Tremblay, and R. Beauvais, "Analysis of macrosegregation in large size forged ingot of high strength steel," in *The 6th International Congress on the Science and Technology of Steelmaking (ICS2015)*, Beijing (China), 2015.

[16] J. D. N. Cheeke, *Fundamentals and applications of ultrasonic waves*. CRC press, 2012.

[17] X. Gros, N. Cameron, and M. King, "Current applications and future trends in phased array technology," *Insight(UK)*, vol. 44, no. 11, pp. 673–678, 2002.

[18] E. Iakovleva, S. Chatillon, P. Bredif, and S. Mahaut, "Multi-mode TFM imaging with artifacts filtering using CIVA UT forwards models," 2014, pp. 72–79.

[19] J. Isla and F. Cegla, "Coded Excitation for Pulse-Echo Systems," *IEEE Transactions on Ultrasonics, Ferroelectrics, and Frequency Control*, vol. 64, no. 4, pp. 736–748, Apr. 2017.

[20] M. H. Pedersen, T. X. Misaridis, and J. A. Jensen, "Clinical evaluation of chirp-coded excitation in medical ultrasound," *Ultrasound in Medicine & Biology*, vol. 29, no. 6, pp. 895–905, Jun. 2003.

## Appendix A: Notch imaging in a 765 mm thick block

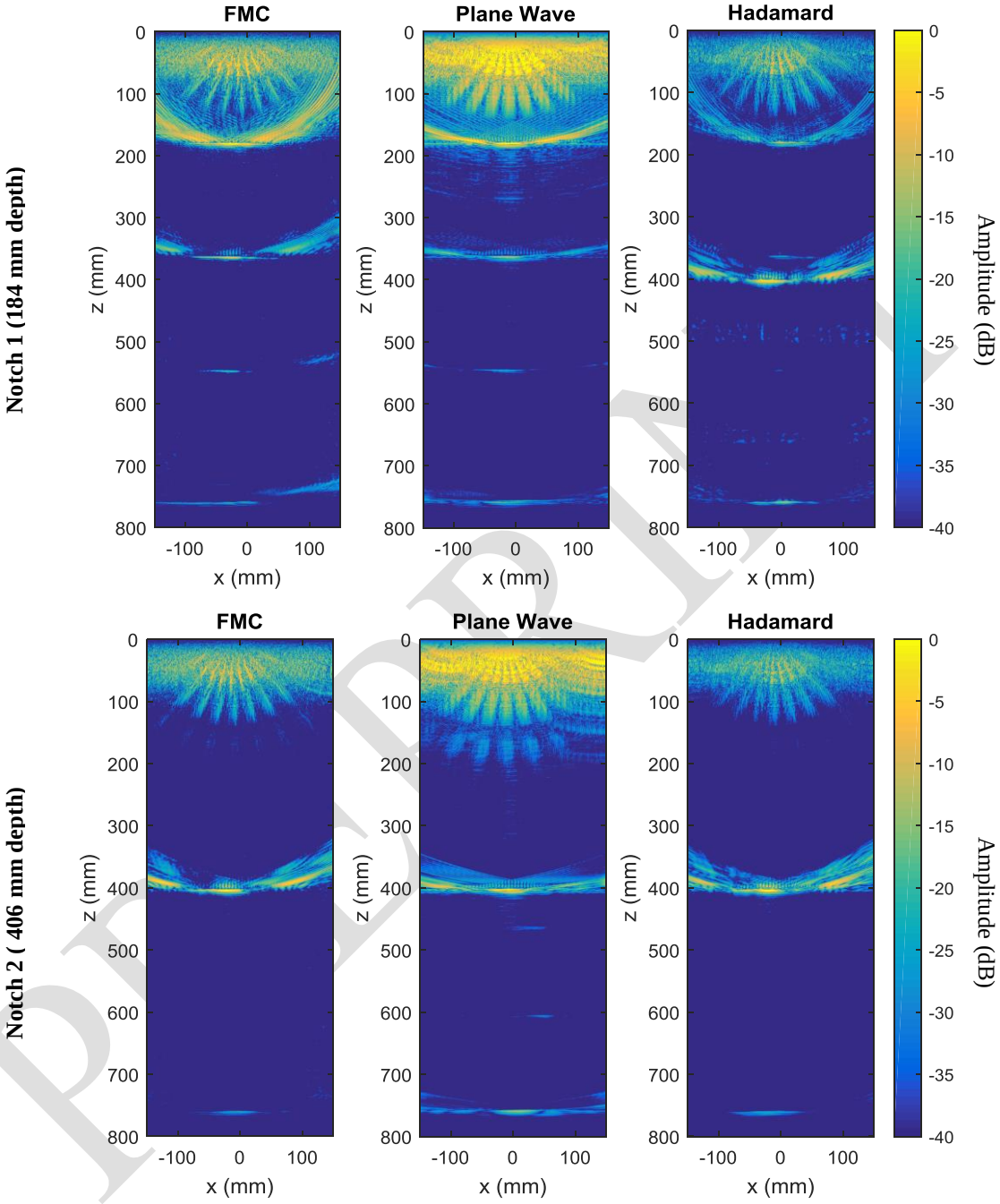

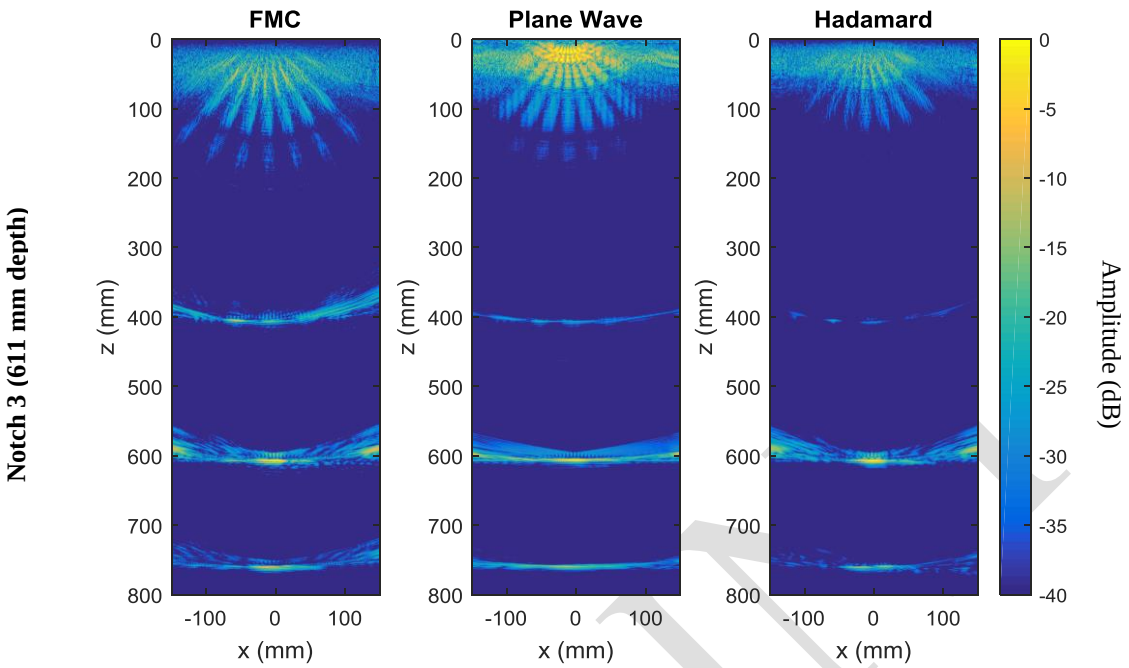
Notch 3 (611 mm depth)
FMC
Plane Wave
Hadamard
z (mm)
x (mm)
Amplitude (dB)
0
100
200
300
400
500
600
700
800
-100
0
100
-5
-10
-15
-20
-25
-30
-35
-40